Proc. Natl. Acad. Sci. USA
Vol. 79, pp. 2559–2563, April 1982
Biophysics

Electron–electron double resonance and saturation-recovery studies of nitroxide electron and nuclear spin-lattice relaxation times and Heisenberg exchange rates: Lateral diffusion in dimyristoyl phosphatidylcholine

(bimolecular collision rates/spin labels/electron paramagnetic resonance)

CAROL A. POPP AND JAMES S. HYDE

National Biomedical ESR Center, Department of Radiology, The Medical College of Wisconsin, 8701 Watertown Plank Road, Milwaukee, Wisconsin 53226

Communicated by Harden M. McConnell, January 22, 1982

ABSTRACT **Lateral diffusion constants of the stearic acid nitroxide radical spin label 2-(14-carboxytetradecyl)-2-ethyl-4,4-dimethyl-3-oxazolindinyl oxide in dispersions of dimyristoyl phosphatidylcholine have been measured. Electron–electron double resonance methods were used to determine the product of the bimolecular collision frequency and T_{1e}, the electron spin-lattice relaxation time. T_{1e} in turn was measured by the technique of saturation recovery. The theoretical model of Träuble and Sackmann was then used to relate the bimolecular collision frequencies to the diffusion constants. Results are in agreement with other methods. Lower spin-label concentrations than were used in previous electron paramagnetic resonance studies are needed (label-to-lipid ratio < 0.5 mol%). Analysis of the data also yields values of the nitrogen nuclear spin-lattice relaxation time of the nitroxide moiety. These values are indicative of membrane fluidity.**

Lateral diffusion is considered to be important for a broad range of biological functions (1, 2, 3), and a variety of techniques have been used for measuring lateral diffusion constants, D. A summary of results obtained from various methods is included in the discussion by Kuo and Wade (4). There is general agreement that D for lipid in membranes above the phase transition temperature falls within the range 10^{-9} to 10^{-7} cm^2 s^{-1}.

Early EPR studies of lateral diffusion in membranes were carried out by Devaux and McConnell (5) and Sackmann and Träuble (6–8) and were based on Heisenberg exchange effects on nitroxide spin-label linewidths. The latter authors made simulations of linewidths to obtain Heisenberg exchange rates, W_{Hex}, from which diffusion constants were calculated. Both studies used high spin-label concentrations and may have been complicated by structural perturbations by the probe molecules. Sackmann and Träuble's results may also have been affected by inhomogeneous broadening from coupling to protons of the spin label and by electron–electron dipolar interactions between spin labels.

We present here the use of electron–electron double resonance (ELDOR) (9) and saturation-recovery (10) techniques to study lateral diffusion in model membranes. ELDOR and saturation-recovery methods permit determination of the Heisenberg exchange rate, which is effectively the bimolecular collision frequency. When this frequency is determined by simple translational diffusion, the lateral diffusion constant can be calculated from the theory of Träuble and Sackmann (8). As will become apparent, much lower values of W_{Hex} can be measured than are possible from analysis of linewidths, thus permitting the use of lower spin-label concentrations.

Our method for determining W_{Hex} differs from EPR spin-label linewidth studies in the following ways. Both ELDOR and saturation-recovery require saturation of the spin system—i.e., the application of large incident microwave fields. They also require the use of microwave cavities that can support two microwave fields simultaneously, with one field used to saturate the spin system at a given transition and the other field used to observe the response of the spin system either at the same transition (saturation-recovery) or at a different transition (ELDOR). Finally, the experimental results are a direct function of spin-lattice relaxation mechanisms, in contrast to more commonly employed spin-label methods that are dependent on transverse relaxation processes.

In the present work, steady-state field-swept in-phase absorption ELDOR methods were used (9). The sample is simultaneously irradiated with two microwave fields of differing frequencies with one at saturating power levels, P_p. When the magnetic field, B, is swept through an observed transition, transfer of saturation can occur from a simultaneously saturated transition, resulting in a decreased intensity of the observed transition. This decrease in signal intensity yields the ELDOR reduction R and is defined as [(signal with pump off) − (signal with pump on)]/(signal with pump off).

The ELDOR reduction can be shown to depend on the ratios W_n/W_e and $W_{Hex}/6W_e$, in which W_n, W_e, and W_{Hex} are the nuclear and electron spin-lattice relaxation and Heisenberg exchange rates, respectively. Nuclear relaxation is induced by motional modulation of electron–nuclear dipolar (END) interactions, which are intramolecular and therefore independent of concentration, whereas W_{Hex} is proportional to concentration. Thus by performing ELDOR experiments at different concentrations, both W_n/W_e and W_{Hex}/W_e can be determined.

Nuclear relaxation and Heisenberg exchange processes couple the hyperfine transitions, increasing the effective number of relaxation pathways (11). For an observing frequency, ν_o, set on the $M_I = 0$ transition while microwave power at ν_p saturates the $M_I = +1$ transition, nuclear transitions to the $M_I = 0$ state result in an effective transfer of saturation and reduction of the $M_I = 0$ signal intensity. For Heisenberg exchange, collision of molecules belonging to the saturated $M_I = +1$ manifold with $M_I = 0$ molecules can result in exchange of spin states and again a transfer of saturation to the $M_I = 0$ transition.

In Fig. 1*a*, stick spectra describing the ELDOR experiment are given (12). The saturating pump field is set at a frequency

The publication costs of this article were defrayed in part by page charge payment. This article must therefore be hereby marked "*advertisement*" in accordance with 18 U. S. C. §1734 solely to indicate this fact.

Abbreviations: ELDOR, electron–electron double resonance; END, electron–nuclear dipolar; rf, radio frequency; 16-SASL, 2-(14-carboxytetradecyl)-2-ethyl-4,4-dimethyl-3-oxazolindinyl oxide (16 stearic acid spin label); Myr$_2$-PtdCho, dimyristoyl phosphatidylcholine.

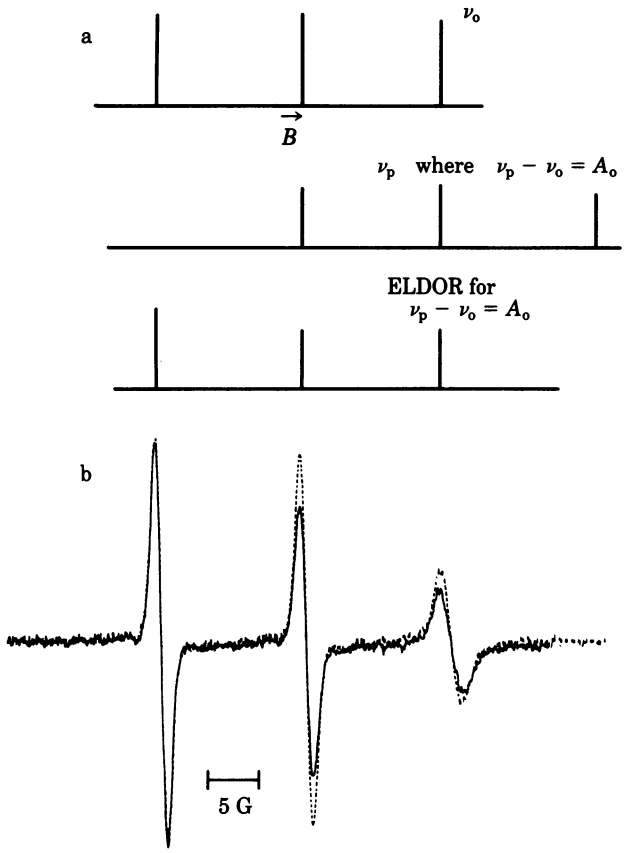

FIG. 1. (*a*) Stick spectra of the signal when the observing field is detected and the pump field is off (*Top*), the pump field is detected (*Middle*), and the ELDOR spectrum is obtained for $\nu_p - \nu_o = A_o$ (*Bottom*). (*b*) Field-swept, in-phase absorption ELDOR spectra of 0.00075 mole ratio 16-SASL/Myr_2-PtdCho for $\nu_p - \nu_o = 40$ MHz with P_p off (broken line) and $P_p = 150$ mW (solid line).

higher than the nonsaturating observing field by an amount equal to the isotropic hyperfine coupling constant, A_o. When B is swept through the resonance condition for the $M_I = 0$ transition, the $M_I = +1$ transition is simultaneously saturated and transfer of saturation can occur from the $M_I = +1$ to the $M_I = 0$ transition. The $M_I = 0$ transition is similarly saturated when the $M_I = -1$ transition is induced by the observing radio frequency (rf) field. No transition is saturated when the $M_I = +1$ transition is induced by the observing rf field, no transfer of saturation can occur, and no ELDOR reduction in signal intensity is seen.

Saturation-recovery techniques can be used to measure W_e (10, 13, 14). In this method, the spin system is first saturated with a pulsed (5-μs) microwave field. The recovery from saturation is then observed with a weak microwave field. Under appropriate conditions, the recovery is characterized by an exponential decay, with the time constant for the decay given by the pure electron spin-lattice relaxation time, $T_{1e} = (2W_e)^{-1}$. These values of W_e can be used in conjunction with the ELDOR data to calculate W_n and W_{Hex}.

Determination of W_{Hex} yields a measure of the bimolecular collision rate and therefore also of the rate of lateral diffusion. In order to compare our studies to those based on other methods, we need to calculate the lateral diffusion constant, D.

The Heisenberg exchange rate can be expressed as $\nu_{enc} \times P$, in which ν_{enc} is the frequency of encounter between two nitroxide radicals and P is the probability for spin exchange upon encounter. Träuble and Sackmann have derived Eq. 1, which relates W_{Hex} to the lateral diffusion constant in a membrane.

$$W_{Hex} = 4d_c \frac{C}{1 + C} \frac{1}{F} \frac{D}{\lambda} P, \quad [1]$$

in which F = area occupied by one lipid molecule, d_c = critical distance for Heisenberg exchange to occur, λ = length of one jump or the lattice constant, and C = mole ratio of spin label to phospholipid (8). This equation is valid when there are no complicating processes such as lateral phase separations.

MATERIALS AND METHODS

Chemicals. 2-(14-Carboxytetradecyl)-2-ethyl-4,4-dimethyl-3-oxazolidinyl oxide (16-SASL; 16 stearic acid spin label) was obtained from Syva (Palo Alto, CA) and dimyristoyl phosphatidylcholine (Myr_2-PtdCho) from Sigma.

Sample Preparations. The spin label and 10 mg of phospholipid dissolved in chloroform were mixed at an appropriate mole ratio and dried under a stream of nitrogen. The dried lipid was dispersed in 20 μl of 0.01 M KH_2PO_4/NaOH buffer by Vortex mixing above the phase transition temperature. The lipid dispersions were transferred to a capillary made from a methylpentene polymer, TPX, and placed within the microwave cavity under a stream of nitrogen at 57°C for approximately 45 min, which was about twice the time needed for the ELDOR reduction to be no longer affected by atmospheric oxygen. The samples were equilibrated with N_2 because the presence of oxygen can lead to inaccurate results in ELDOR and other EPR studies due to O_2-dependent shortening of the nitroxide electron T_{1e} (15).

Instrumentation. ELDOR spectra were obtained by using a Varian E800 ELDOR bridge with a Varian E101 microwave bridge. A new cavity similar to that used in the original studies (figure 2 of ref. 9) was designed and built. The cavity supports orthogonal rectangular TE_{103} and TE_{102} modes with the TE_{103} mode used as a pump mode and the TE_{102} used as the observing mode. Insertion of a Teflon screw into the unshared portion of the TE_{103} mode allowed the pump frequency to be changed by 200 MHz. Cross coupling between modes was minimized by the use of two reactive paddles at the junction between the TE_{102} mode and the unshared portion of the TE_{103}. Because of the good isolation between modes, the high-quality factor, Q, cylindrical cavity that is employed in the commercial apparatus as a filter of pump microwaves that leak into the observing mode was removed with a resultant increase in signal-to-noise ratio of about a factor of 2.

ELDOR Measurements. The same TPX capillary was used for all measurements and the samples were carefully positioned within the cavity. The frequency difference between modes was set with a frequency counter to $\nu_p - \nu_o = +40$ MHz. A Hewlett–Packard power meter connected to the pump arm with a cross-guide coupler was used to measure the incident microwave power of the pump mode. The choice of pump powers needed to obtain values of ELDOR reduction required a compromise between high powers that gave large values of R but significant heating of these lossy samples and low powers that gave smaller values of R but fewer problems from heating. Typically, 12 power settings were used with one at 39-decibel pump power and 11 between 100- and 200-mW incident power. ELDOR reductions were obtained from the average of usually three scans of the spectra. The spectra were normalized to the low-field peak-to-peak height. No ELDOR transfer of saturation is induced with this transition, and this peak can therefore be used as an internal control on experimental variations of, for example, sample position and temperature. The low-field peak-to-peak height varied during an experiment usually by 1% or 2%.

Table 1. ELDOR results

Temp., °C	C, mole ratio 16-SASL/ Myr_2-PtdCho	τ_R^B,* s × 10^{10}	τ_R^C,* s × 10^{10}	R_∞^{-1}†	$b = W_n/W_e$‡	$b'' = W_{Hex}/6W_e$§
27	0.00075	9.79 ± 0.02	8.61 ± 0.01	1.14 ± 0.13	13.80	
	0.0050			1.15 ± 0.12		
37	0.00075	7.31 ± 0.02	5.86 ± 0.05	1.53 ± 0.08	3.60	
	0.0025			1.49 ± 0.08		0.15
47	0.00075	5.39 ± 0.06	4.05 ± 0.06	1.96 ± 0.08	1.69	
	0.0025			1.80 ± 0.09		0.20
57	0.00075	2.79 ± 0.04	1.75 ± 0.05	2.31 ± 0.09	1.18	
	0.0025			1.98 ± 0.08		0.25

* Isotropic rotational correlation times calculated by using magnetic parameters for 2-(3-carboxypropyl)-4,4-dimethyl-2-tridecyl-3-oxazolidinyl oxide (16, 17). Errors refer to standard deviations of multiple experiments.
† Errors refer to least-squares analysis errors.
‡ Calculated by using Eq. 2.
§ Calculated by using Eq. 4.

The temperature was controlled with the Varian variable temperature accessory equipment and measured to within ±1°C with a copper/constantan thermocouple and a Fluke 2190A digital thermometer. Estimated temperature change over the range of pump powers needed for measurement of R was no more than ±1°C.

Except where noted, the magnitude of the observing field was less than half the rf field needed to maximize the signal intensity. The amplitudes of the 100-kHz and 10-kHz modulation fields were sufficiently low that no line broadening was evident.

Saturation-Recovery Studies. Equipment (14) and methods are based on work of Huisjen and Hyde (10). The saturation-recovery decays were detected with a weak, 3-mW incident power, observing field. The pump field power was 100 mW. A pulse width of 5 μs was used with a repetition rate of 25 kHz. The pump field was phase modulated at 50 Hz to suppress free-induction decay, and 25-Hz field modulation with 1.2-G amplitude was employed to improve instrument stability. Data accumulation was obtained with a 40-ns aperture and 512 channels. Approximately 4 × 10^6 accumulations were obtained.

EXPERIMENTAL

The EPR and field-swept ELDOR spectra of a nitrogen-equilibrated, aqueous dispersion of 0.00075 mole ratio 16-SASL/Myr_2-PtdCho at 37°C are shown in Fig. 1*B*. Rotational correlation times for 0.00075 mole ratio 16-SASL/Myr_2-PtdCho, in which τ_R^B and τ_R^C are τ_R values calculated from the linear and quadratic terms of $T_2^{-1} = A + BM_I + CM_I$ (T_2 is the transverse relaxation time), are shown in Table 1 (16).

The ELDOR reduction, R, is a function of a variety of experimental conditions, which include the magnitude of incident pump rf field, modulation field, deviation of frequency difference from A_o, etc. (18, 19). R becomes independent of these factors when it is extrapolated to infinite pump power. Fig. 2 shows plots of R^{-1} vs. P_p^{-1} for ν_o:$M_I = 0$, ν_p:$M_I = +1$. The plots show the expected linear dependence of R_∞^{-1} on P_p^{-1}. Values of R_∞^{-1} for 0.00075, 0.0025, and 0.0050 mole ratio 16-SASL/Myr_2-PtdCho are given in Table 1. Measurements of R_∞^{-1} for 0.0050 mole ratio 16-SASL/Myr_2-PtdCho at 47°C were independent of field modulation frequency (either 10 or 100 kHz) and observing power levels (either ½ or ¼ of that power required for maximal signal intensity).

Although Heisenberg exchange has the same ELDOR effect for all pairs of coupled transitions, the END mechanism leads to different values of R_∞. When the $M_I = 0$ transition is observed as the $M_I = +1$ transition is saturated, it can be shown (9) that

$$R_\infty(\text{END}) = \left[\frac{b + b^2}{1 + 3b + b^2}\right]; \quad [2]$$

$$R_\infty(\text{Heisenberg exchange}) = \left[\frac{b''}{1 + b''}\right]; \quad [3]$$

and

$$R_\infty(\text{END + Heisenberg exchange}) = \left[\frac{(b + b'')(b + 3b'' + 1)}{(1 + 3b'')(1 + b'') + b(b + 4b'' + 3)}\right]; \quad [4]$$

$$b = W_n/W_e;\ b'' = W_{Hex}/6W_e. \quad [5]$$

Using Eq. 2, W_n/W_e was calculated from R_∞ for samples of lowest spin-label concentration, 0.00075 mole ratio. Knowing b, it was then possible to calculate b'' from Eq. 4 (see Table 1).

Saturation-recovery studies have been carried out, and the decay and semilogarithmic plots from the $M_I = 0$ transition of 0.0025 mole ratio sample at 27°C are shown in Fig. 3*A*. The decay is characterized by an exponential function. No M_I dependence has been seen. The temperature dependence of T_{1e} is shown in Fig. 3*b*.

Because the concentration dependence of W_e is small, with W_e varying minimally over a factor of 10 change in spin-label

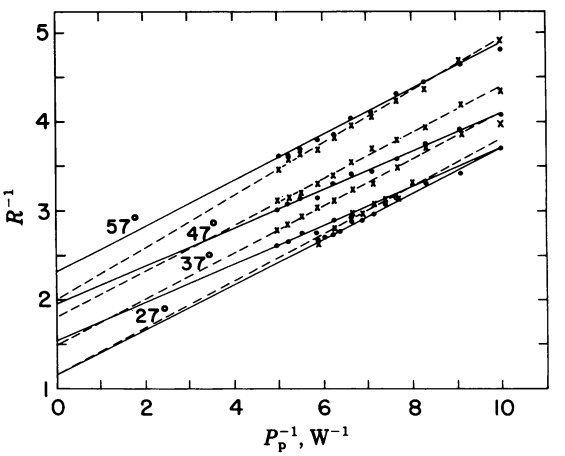

FIG. 2. R^{-1} vs. P_p^{-1} for 0.00075 (●) and 0.0025 (×) mole ratio 16-SASL/Myr_2-PtdCho at 37, 47, and 57°C and 0.00075 (●) and 0.0050 mole ratio (×) at 27°C. Each point was obtained from multiple scans of the spectrum. See text for details.

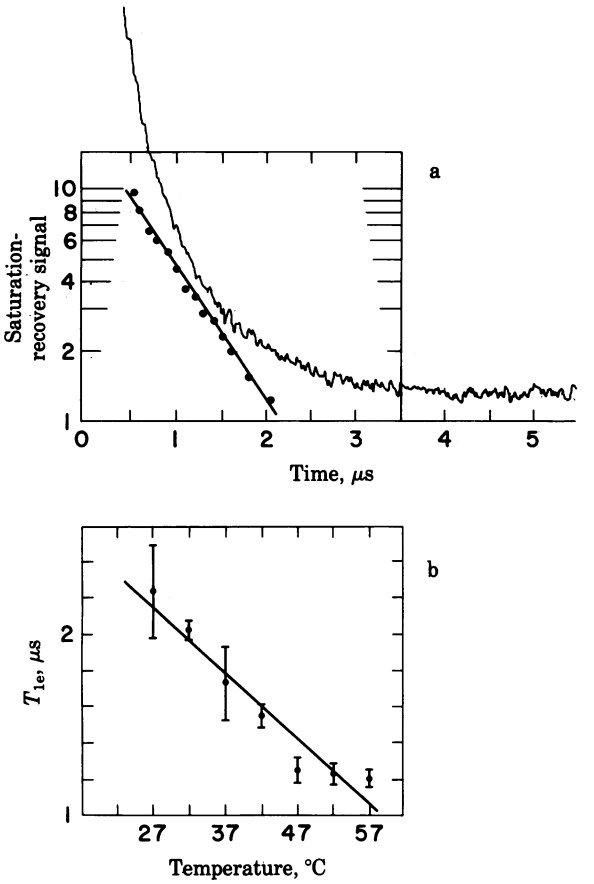

FIG. 3. (*a*) Saturation-recovery decay and semilogarithmic plot of the decay for the $M_I = 0$ transition for 0.0025 mole ratio 16-SASL/Myr_2-PtdCho at 27°C. (*b*) Temperature dependence of T_{1e} obtained from these decays.

concentration, we inserted the data of Fig. 3*b* into Eq. 5 to calculate W_n and W_{Hex} (Tables 2 and 3).

ANALYSIS AND DISCUSSION

Electron Spin-Lattice Relaxation. The electron spin-lattice relaxation rate W_e has been described as a function of *g*-tensor and hyperfine interactions and using the expressions given by Kivelson (20) with $M_I = 0$

$$W_e = \frac{1}{2}\left\{\frac{7I(I+1)}{8}\left[\left(\frac{1}{5}\right)\left(\frac{4\pi}{3}\right)\left(A_z - \frac{1}{2}(A_x + A_y)\right)\right]^2 + \frac{1}{3}\left[\left(\frac{\beta}{h}\right)\left(g_z - \frac{1}{2}(g_x + g_y)\right)\right]^2 \frac{B_o^2}{5}\right\}\left(\frac{\tau_R}{1 + \omega_o^2\tau_R^2}\right) \quad [6]$$

and as a function of the spin rotation mechanism (9)

$$W_e = \sum_i \frac{(g_i - g_e)^2}{18}\left(\frac{1}{\tau_R}\right), \quad [7]$$

in which A_i = principal values of the hyperfine tensor, g_i = principal components of the *g*-tensor, g_e = electron *g* values, ω_o = electron Larmor frequency, B_o = magnetic field at resonance, and τ_R = isotropic rotational correlation time. For $\omega_o\tau_R \gg 1$, as is the case for these studies, $W_e \propto \tau_R^{-1}$ and W_e will increase with increasing temperature (Fig. 2).

Values for W_e calculated from Eq. 6 and 7, by using $\tau'_R = (\tau_R^B + \tau_R^C)/2$ are shown in Table 2. These values are two orders of magnitude smaller than the saturation-recovery data.

At higher temperatures, where the nuclear and electron spin-lattice relaxation rates have similar magnitudes, the saturation-recovery time constant can, in principle, be somewhat shorter than the true T_{1e} (21). One might also question the validity of the application of Eq. 6 to a problem in which the motion must certainly be anisotropic. However, it seems quite impossible to account in these ways for the discrepancy of two orders of magnitude, and we therefore conclude that there is uncertainty in our understanding of the dominant spin-lattice relaxation mechanism. It is noted that Percival and Hyde (13) report similar values of T_{1e} at similar correlation times for a nitroxide diffusing in an isotropic fluid.

Nuclear Spin-Lattice Relaxation. The nitroxide ^{14}N nuclear spin-lattice relaxation rate, W_n, is a function of the END interaction

$$W_n = \frac{4\pi^2}{10}\left\{\left[\left(\frac{6^{1/2}}{4}\right)(A_z - A_o)\right]^2 + 2\left[\frac{1}{4}(A_x - A_y)\right]^2\right\}\left(\frac{\tau_R}{1 + \omega_n^2\tau_R^2}\right), \quad [8]$$

in which A_o = isotropic hyperfine constant and ω_n = nuclear Larmor frequency (9, 11). Because $\omega_n/\omega_o = 1/900$, $\omega_n\tau_R << 1$ and W_n will increase with decreasing temperature (Table 2). W_n^{iso} was calculated by using Eq. 8 and τ'_R and is shown in Table 2. Calculated values for W_n^{iso} are a factor of ½ to ¼ lower than obtained from ELDOR and saturation-recovery experiments, W_n^{ELDOR}.

Calculations of τ_R^B and τ_R^C suggest, however, that an isotropic rotational diffusion model is inadequate. This analysis neglects any complicated motions such as restricted "wobble." Although there is uncertainty in τ_R, we cannot rule out the possibility that there is some inadequacy in our understanding of motional modulation of electron–nuclear interactions.

Heisenberg Exchange Rates. Using Träuble and Sackmann's diffusional model and their values for structural parameters for membranes (8), the lateral diffusion constants *D* were calculated from Eq. 1 and are given in Table 3. Our results for *D* are in good agreement with values obtained by using other methods (4).

Previous methods for measuring W_{Hex} in membranes relied on linewidth measurements. There are two significant complications in linewidth studies: inhomogeneous broadening and electron–electron dipolar interactions.

A commonly employed equation for calculating the Heisenberg exchange rate from experimentally determined linewidths is

$$W_{Hex} = \frac{3^{3/2}\gamma}{4}(\Delta B_{pp} - \Delta B_{pp}^o), \quad [9]$$

in which ΔB_{pp} is the derivative peak-to-peak linewidth in the presence of Heisenberg exchange and ΔB_{pp}^o is the linewidth in the absence of exchange (22). γ is the magnetogyric ratio. The

Table 2. Electron and nuclear spin relaxation rates

Temp., °C	$W_e^{g \text{ and hf}}$,* $s^{-1} \times 10^{-4}$	W_e^{SR},† $s^{-1} \times 10^{-4}$	W_n^{ELDOR},‡ $s^{-1} \times 10^{-6}$	W_n^{iso},§ $s^{-1} \times 10^{-6}$
27	0.68	0.34	20.0	3.6
37	0.95	0.48	6.3	2.6
47	1.32	0.66	3.8	1.9
57	2.75	1.38	3.5	0.9

Units for all W_e are angular frequency.
* Calculated from Eq. 6.
† Calculated from Eq. 7.
‡ Experimental values calculated by using the analysis of this paper.
§ Calculated from Eq. 8.

Table 3. Lateral diffusion rates

Temp., °C	W_{Hex}, $s^{-1} \times 10^{-6}$	D, $cm^2\ s^{-1} \times 10^8$
37	0.25	5.8
47	0.43	10.0
57	0.68	15.8

use of this equation requires the assumption that the lines are homogeneously broadened. In the presence of inhomogeneous broadening from, for example, unresolved proton hyperfine coupling, large errors in estimating W_{Hex} can occur (22). The presence of inhomogeneous broadening should not affect our ELDOR results (19).

Electron–electron dipolar interactions lead to linewidth contributions that must be accounted for to obtain Heisenberg exchange rates from conventional line shape analysis. These dipolar linewidth contributions are dominated by the secular terms of the dipolar Hamiltonian (23) and must be obtained by using computer simulations that are complicated by the need for an appropriate motional model. ELDOR and saturation-recovery results should not be affected by these secular terms. T_{1e}, which can be shortened by nonsecular ($S_1^{\pm}S_{2Z} + S_{1Z}S_2^{\pm}$) terms, is measured directly by saturation-recovery methods and thus no errors are introduced in the determination of W_{Hex}. However, pseudosecular ($S_1^{\pm}S_2^{\mp}$) terms of the dipolar Hamiltonian lead to coupling of the hyperfine transitions that are not easily distinguished from couplings induced by Heisenberg exchange (24). It is an interesting problem in physical chemistry to separate pseudosecular and Heisenberg exchange interactions, but for our present purposes the physical origin of the intermolecular interactions that couple transitions is of relatively little significance. The primary effect would be to alter the magnitude of the interaction distance (d_c in Eq. 1), which is in any event somewhat uncertain.

CONCLUDING REMARKS

Presently our methods for measuring W_{Hex} in membranes are limited by the relatively fast nuclear spin relaxation, which is an additional and effective ELDOR-active mechanism. The fast nuclear relaxation is particularly troublesome in these studies because the nuclear relaxation increases as W_{Hex} decreases. (Thus, we are unable to measure W_{Hex} at 27°C, using low concentrations of spin labels.) A method to alleviate this problem would be the simultaneous use of ^{14}N and ^{15}N spin labels to eliminate nuclear spin transitions that couple observed and saturated EPR transitions.

Our calculations of lateral diffusion constants from W_{Hex} can have errors arising from the model dependence of Eq. 1 and the need for membrane structural data. However, our purpose in calculating D was to compare our method with other techniques, and we find our data to be in good agreement (4). W_{Hex} is in itself a useful parameter of lateral diffusion.

We have demonstrated that lower rates of Heisenberg exchange can be measured with ELDOR than is possible from analysis of the effects of exchange on lineshapes. Thus, lower spin-label concentrations can be employed, thereby decreasing the risk of structural perturbations by the spin-label probes. Additionally, it appears feasible with ELDOR to measure translational diffusion below the main phase transition, where the diffusion constant is presumably rather small.

Rotational diffusion can now be studied in two ways, namely linewidth and nitrogen nuclear relaxation analyses. Although our "window" for rotational correlation times from W_n is only about two orders of magnitude compared with four orders for lineshape studies, W_n data are still interesting. Motional modulation of the END interaction can be expected to determine both linewidth and W_n, and it is hoped that their independent measurement will contribute to development of an improved motional model.

A number of competing methods for measuring translational diffusion require specialized membrane geometries, viz, the use of oriented films. The present experiments have been carried out with simple lipid dispersions, which we think will be of considerable convenience in manipulating lipid and medium compositions in order to learn about translational diffusion in membranes in greater detail.

This work was supported in part by Grants GM-22923, GM-27665, and RR-01008 from the National Institutes of Health.

1. Rubenstein, J. L. R., Smith, B. A. & McConnell, H. M. (1979) *Proc. Natl. Acad. Sci. USA* **76**, 15–18.
2. Schindler, M., Koppel, D. E. & Sheetz, M. P. (1980) *Proc. Natl. Acad. Sci. USA* **77**, 1457–1461.
3. Derzko, Z. & Jacobson, K. (1980) *Biochemistry* **19**, 6050–6057.
4. Kuo, A. K. & Wade, C. G. (1979) *Biochemistry* **18**, 2300–2308.
5. Devaux, P. & McConnell, H. M. (1972) *J. Am. Chem. Soc.* **94**, 4475–4481.
6. Sackmann, E. & Träuble, H. (1972) *J. Am. Chem. Soc.* **94**, 4482–4491.
7. Sackmann, E. & Träuble, H. (1972) *J. Am. Chem. Soc.* **94**, 4492–4498.
8. Träuble, H. & Sackmann, E. (1972) *J. Am. Chem. Soc.* **94**, 4499–4510.
9. Hyde, J. S., Chien, J. C. W. & Freed, J. H. (1968) *J. Chem. Phys.* **48**, 4211–4226.
10. Huisjen, M. & Hyde, J. S. (1974) *Rev. Sci. Instrum.* **45**, 669–675.
11. Freed, J. H. (1965) *J. Chem. Phys.* **43**, 2312–2332.
12. Kevan, L. & Kispert, L. D. (1976) *Electron Spin Double Resonance Spectroscopy* (Wiley, New York).
13. Percival, P. W. & Hyde, J. S. (1976) *J. Magn. Reson.* **23**, 249–257.
14. Forrer, J. E., Wubben, R. C. & Hyde, J. S. (1980) *Bull. Magn. Reson.* **2**, 441.
15. Popp, C. A. & Hyde, J. S. (1981) *J. Magn. Reson.* **43**, 249–258.
16. Goldman, S. A., Bruno, G. V., Polnaszek, C. F. & Freed, J. H. (1972) *J. Chem. Phys.* **56**, 716–735.
17. Berliner, L. J. ed. (1976) *Spin Labeling: Theory and Applications* (Academic, New York) Appendix II.
18. Eastman, M. P., Bruno, G. V. & Freed, J. H. (1970) *J. Chem. Phys.* **52**, 321–327.
19. Dalton, L. A., Monge, J. L., Dalton, L. R. & Kwiram, A. L. (1974) *Chem. Phys.* **6**, 166–182.
20. Kivelson, D. (1960) *J. Chem. Phys.* **33**, 1094–1106.
21. Freed, J. H. (1974) *J. Phys. Chem.* **78**, 1155–1167.
22. Bales, B. L. (1980) *J. Magn. Reson.* **38**, 193–205.
23. Abragam, A. (1961) *The Principles of Nuclear Magnetism* (Clarendon, Oxford).
24. Freed, J. H. (1979) in *Multiple Electron Spin Resonance Spectroscopy*, eds. Dorio, M. M. & Freed, J. H. (Plenum, New York), pp. 73–142.